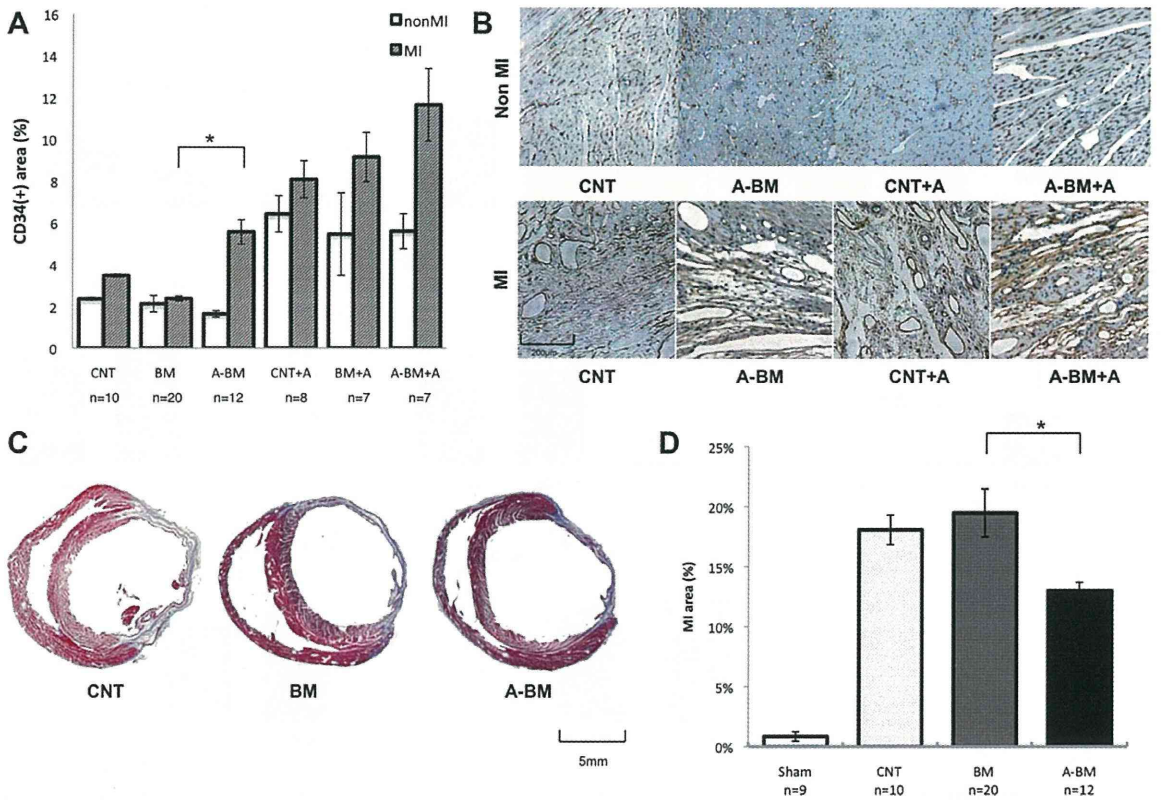

Figure 7. Effect of bone marrow-derived mesenchymal stem cell (BM-MSC) transplantation and/or treatment with candesartan on vessel density and infarction size in the heart in vivo. **(A):** The percentage of CD34 positive area in control myocardial infarction (MI) (CNT), MI with bone candesartan-pretreated BM-MSCs transplantation (BM), candesartan-pretreated BM (A-BM), and additional oral administration of candesartan after the transplantation (CNT+A, BM+A, A-BM+A) are calculated and averaged. **(B):** Representative microscopic image of immunohistochemistry using anti-CD34 antibody to detect vessels at center of MI zone and peri-MI normal zone (non-MI) are shown. Scale bar = 20 μm. Pretreatment with candesartan significantly increased vessel density at MI zone; on the other hand, oral administration of candesartan significantly increased vessel density at non-MI zone. **(C):** Representative masson-trichrom staining of the heart at the tendinous cord level of CNT, BM, and A-BM are shown. The digitized data were measured and calculated in **(D)**. By the candesartan-pretreatment, BM-MSC transplantation significantly decreased in percentage fibrosis volume. Scale bar = 5 mm. *p<0.05. Abbreviations: BM, bone marrow; CNT, control; MI, myocardial infarction.

incidence of cardiomyogenic transdifferentiation of human BM-MSCs is extremely rare, it has been impossible to statistically analyze the effect on CTE of various drugs or interventions in vivo. Therefore, there has been no systematic strategy for improvement of CTE of BM-MSCs until our previous article [6, 9–11, 19]. Our in vivo model of ARB-treated BM-MSCs is able to statistically analyze the effects of drugs on CTE, which is important for further improvement of CTE. In vitro, the pioglitazone's effect on CTE was independent from the effect of ARB; therefore, the additional administration of pioglitazone, as a PPAR-γ activator may be expected to improve CTE further. Further experiments should be done.

Study Limitation

In our previous study, we have used BM-MSCs obtained from a 41-year-old and a 90-year-old men. The CTE results were 1% and 0.3% in vitro [19], respectively. In this study, the CTE of default BM-MSCs from neonates was approximately 3%–5%. This data implies BM-MSCs obtained from younger generations that may have higher cardiomyogenic transdifferentiation ability. As ARB is known to have a potential for an anti-aging effect, the effect of ARB on BM-MSCs might increase the CTE by ARB's anti-aging effect on BM-MSCs. Further experiments should be done on this issue.

In vivo MI model was performed by two series (Sham, CNT, BM, A-BM series and CNT-A, BM-A, A-BM-A series) at different periods. As it was difficult to control the size of the MI at the coronary ligation, the size of the MI of later series are slightly larger (N.S.) than the former series. Therefore, we did not perform statistical analysis on some parameters between the series (separated by dotted line in the figures). The serum BNP level and the size of percentage MI volume are slightly larger in the later series. In this study, intra-individual difference values were compared with the values of the two series.

Conclusion

Pretreatment with angiotensin receptor blockers (ARBs) in culture activate human marrow-derived mesenchymal stem cells by angiotensin-II receptor type 1 blockade. ARBs-pretreated human marrow-derived msenchymal stem cells was significantly improved cardiomyogenic transdifferentiation efficiency in vitro and in vivo, and transplantation of the ARBs-pretreated cells significantly improved cardiac function and can be a promising cardiac stem cell source from which to expect cardiomyogenesis.

Acknowledgments

The research was partially supported by a grant from the Ministry of Education, Science and Culture, Japan. A part of this work was undertaken at the Keio Integrated Medical Research Center.

Disclosure of Potential Conflicts of Interest

The authors indicate no potential conflicts of interest.

References

1 Boheler KR, Czyz J, Tweedie D et al. Differentiation of pluripotent embryonic stem cells into cardiomyocytes. Circ Res 2002;91:189–201.
2 Makino S, Fukuda K, Miyoshi S et al. Cardiomyocytes can be generated from marrow stromal cells in vitro. J Clin Invest 1999;103:697–705.
3 Orlic D, Kajstura J, Chimenti S et al. Bone marrow cells regenerate infarcted myocardium. Nature 2001;410:701–705.
4 Tomita S, Li RK, Weisel RD et al. Autologous transplantation of bone marrow cells improves damaged heart function. Circulation 1999;100:II247–II256.
5 Asahara T, Murohara T, Sullivan A et al. Isolation of putative progenitor endothelial cells for angiogenesis. Science 1997;275:964–967.
6 Tsuji H, Miyoshi S, Ikegami Y et al. Xenografted human amniotic membrane-derived mesenchymal stem cells are immunologically tolerated and transdifferentiated into cardiomyocytes. Circ Res 2010;106:1613–1623.
7 Terai M, Uyama T, Sugiki T et al. Immortalization of human fetal cells: The life span of umbilical cord blood-derived cells can be prolonged without manipulating p16INK4a/RB braking pathway. Mol Biol Cell 2005;16:1491–1499.
8 Takeda Y, Mori T, Imabayashi H et al. Can the life span of human marrow stromal cells be prolonged by bmi-1, E6, E7, and/or telomerase without affecting cardiomyogenic differentiation? J Gene Med 2004;6:833–845.
9 Hida N, Nishiyama N, Miyoshi S et al. Novel cardiac precursor-like cells from human menstrual blood-derived mesenchymal cells. Stem Cells 2008;26:1695–1704.
10 Nishiyama N, Miyoshi S, Hida N et al. The significant cardiomyogenic potential of human umbilical cord blood-derived mesenchymal stem cells in vitro. Stem Cells 2007;25:2017–2024.
11 Okamoto K, Miyoshi S, Toyoda M et al. 'Working' cardiomyocytes exhibiting plateau action potentials from human placenta-derived extraembryonic mesodermal cells. Exp Cell Res 2007;313:2550–2562.
12 Grauss RW, Winter EM, van Tuyn J et al. Mesenchymal stem cells from ischemic heart disease patients improve left ventricular function after acute myocardial infarction. Am J Physiol Heart Circ Physiol 2007;293:H2438–H2447.
13 Hou M, Yang KM, Zhang H et al. Transplantation of mesenchymal stem cells from human bone marrow improves damaged heart function in rats. Int J Cardiol 2007;115:220–228.
14 Chen SL, Fang WW, Ye F et al. Effect on left ventricular function of intracoronary transplantation of autologous bone marrow mesenchymal stem cell in patients with acute myocardial infarction. Am J Cardiol 2004;94:92–95.
15 Hare JM, Traverse JH, Henry TD et al. A randomized, double-blind, placebo-controlled, dose-escalation study of intravenous adult human mesenchymal stem cells (prochymal) after acute myocardial infarction. J Am Coll Cardiol 2009;54:2277–2286.
16 Matsushita K, Wu Y, Okamoto Y et al. Local renin angiotensin expression regulates human mesenchymal stem cell differentiation to adipocytes. Hypertension 2006;48:1095–1102.
17 Iwanami J, Mogi M, Li JM et al. Deletion of angiotensin II type 2 receptor attenuates protective effects of bone marrow stromal cell treatment on ischemia-reperfusion brain injury in mice. Stroke 2008; 39:2554–2559.
18 Ikegami Y, Miyoshi S, Nishiyama N et al. Serum-independent cardiomyogenic transdifferentiation in human endometrium-derived mesenchymal cells. Artif Organs 2010;34:280–288.
19 Shinmura D, Togashi I, Miyoshi S et al. Pretreatment of human mesenchymal stem cells with pioglitazone improved efficiency of cardiomyogenic transdifferentiation and improved cardiac function. Stem Cells 2010 (in press).
20 Kami D, Shiojima I, Makino H et al. Gremlin enhances the determined path to cardiomyogenesis. PLoS One 2008;3:e2407.
21 Gnecchi M, He H, Liang O et al. Paracrine action accounts for marked protection of ischemic heart by Akt-modified mesenchymal stem cells. Nat Med 2005;11:367–368.

See www.StemCells.com for supporting information available online.

Lasers in Surgery and Medicine 43:984–990 (2011)

Myocardial Electrical Conduction Block Induced by Photosensitization Reaction in Exposed Porcine Hearts In Vivo

Arisa Ito, MSc,[1]* Shunichiro Miyoshi, MD,[2] Takehiro Kimura, MD,[2] Seiji Takatsuki, MD,[2] Kotaro Fukumoto, MD,[2] Keiichi Fukuda, MD, PhD,[2] and Tsunenori Arai, PhD[1]

[1]*School of Fundamental Science and Technology, Graduate School of Science and Technology, Keio University, 3-14-1, Hiyoshi, Kohoku-ku, Yokohama 223-8522, Japan*

[2]*Department of Cardiology, Keio University School of Medicine, 35 Shinanomachi, Shinjuku-ku, Tokyo 160-8582, Japan*

Background and Objective: This study proposes photosensitization reaction for non-thermal cardiac ablation in arrhythmia therapy. Acute and chronic phase experiments were conducted in exposed porcine hearts to demonstrate the photosensitization reaction-induced myocardial electrical conduction block *in vivo*.

Study Design/Materials and Methods: The porcine left atrial appendage was exposed under an open-chest procedure. Then, a water-soluble chlorin photosensitizer, NPe6, was injected into the pigs intravenously at 5 or 10 mg/kg. About 15 or 30 minutes after the injection, a 663-nm continuous-wave diode laser was irradiated on the surface of the atrial appendage through a silica optical fiber. The laser energy was delivered to the tissue point by point at an energy density of 50–208 J/cm^2.

Results: Acute and chronic tissue damages as a result of the photosensitization reaction were determined by electrophysiology and histology, respectively. The change in the myocardial conduction time between two electrodes was measured immediately after the completion of the 35-mm irradiation line between the electrodes. The conduction delay of 35.5 milliseconds might be due to the change in the conduction pathway induced by transmural acute conduction block with the photosensitization reaction. The tissue temperature increase in the irradiated area was approximately 12.8°C. Azan-staining revealed about 1-mm transmural fibrosis of the atrial appendage at 2 weeks after the irradiation (50 J/cm^2).

Conclusions: The results suggest that the photosensitization reaction might induce acute and chronic myocardial electrical conduction block. Cardiac ablation with the photosensitization reaction might be a non-temperature-mediated methodology for arrhythmia therapy. Lasers Surg. Med. 43:984–990, 2011.

Key words: arrhythmia; atrial fibrillation; cardiac ablation; NPe6; photodynamic therapy; photosensitizer

INTRODUCTION

The most common curative therapy for atrial tachyarrhythmia is radiofrequency catheter ablation to isolate arrhythmogenic foci [1–3]. The resistive heating of myocardium with radiofrequency energy induces thermal tissue injury in the pathway of ectopic beat conduction, resulting in myocardial electrical conduction block. However, there are several limitations of radiofrequency ablation including thermal complications (total incidence rate, 4–6%), such as thromboembolism and cardiac tamponade [4–6]. Alternative energy sources for cardiac ablation have been developed such as laser ablation, in which the laser energy is absorbed by the myocardium, resulting in temperature rise of tissue [7–9]. However, the laser ablation might face the same problem of the thermal complications as radiofrequency ablation. In spite of the relatively low incident rate of the thermal complications appeared in these thermal ablation therapies, totally beneficial methodologies are required compared to conservative treatment with medication.

We proposed the use of non-temperature-mediated cytotoxic process with photosensitization reaction to create a myocardial electrical conduction block. In clinical practice, photosensitization reaction is applied to a non-invasive cancer therapy known as photodynamic therapy (PDT) using photosensitizer specific accumulation to tumor tissue [10,11]. The photochemical interactions between photons, photosensitizer, and oxygen result in the generation of reactive oxygen species, mainly singlet molecular oxygen [12,13], which induce oxidative damage of biological molecules, resulting in apoptotic or necrotic cell death [14,15]. Since there is no photosensitizer specific accumulation in normal myocardium, particularly short drug–light intervals (approximately one-order shorter than the conventional interval) can be used in the application of photosensitization reaction for myocardial tissue.

Contract grant sponsor: The Japan Science and Technology Agency (Supporting Program for Creating University Ventures); Contract grant number: 1904; Contract grant sponsor: The Japan Society for the Promotion of Science (Research Fellowships for Young Scientists); Contract grant number: 3455.
*Corresponding to: Arisa Ito, MSc, 3-14-1, Hiyoshi, Kohoku-ku, Yokohama 223-8522, Japan. E-mail: arisa@a3.keio.jp
Accepted 19 September 2011
Published online in Wiley Online Library (wileyonlinelibrary.com).
DOI 10.1002/lsm.21136

The aim of this study was to demonstrate the feasibility of the application of photosensitization reaction for non-thermal cardiac ablation. Myocardial electrical conduction block caused by the photosensitization reaction with a water-soluble chlorin photosensitizer was examined electrophysiologically in an acute phase study and histopathologically in a chronic phase study with surgically exposed porcine hearts.

MATERIALS AND METHODS

Animal Preparation

The animal study was conducted with the approval of the Animal Care Committee in Keio University, Japan. LW female pigs weighing about 15 kg (1.5–2 months in age) for the acute phase study and about 24 kg (2–2.5 months in age) for the chronic phase study were sedated by injecting ketamine (2 mg/kg) and xylazine (2 mg/kg) intramuscularly, followed by mask-induced anesthesia with 5% isoflurane and pure O_2 at 1.5–2.0 L/minute. After tracheal intubation, general anesthesia was maintained by inducing inhalation of 2.5% isoflurane and pure O_2 at the same flow rate. The left cervical vein was cannulated for blood sampling. Standard limb-lead II electrocardiogram, heart rate, body temperature, and oxygen saturation by pulse oximetry were monitored continuously throughout the procedure.

Photosensitizer and Laser Light Source for In Vivo Study

A water-soluble chlorin photosensitizer, NPe6 (mono-L-aspartyl chlorin-e6), also known as talaporfin sodium, was used. NPe6 is approved in Japan as Laserphyrin® (Meiji Seika Kaisha, Ltd, Tokyo, Japan) for the treatment of early stage bronchopulmonary cancer [16]. This photosensitizer has a molecular weight of 799.69 and a significant absorption peak in the Q band at 664 nm [16–18]. NPe6 has a strong molar absorption coefficient of $4.0 \times 10^4\ M^{-1}\ cm^{-1}$ and a high quantum yield of singlet oxygen generation of 0.77 with the absorption peak in the Q band [18]. A 663-nm red diode laser was employed as a light source to excite NPe6 at the Q band. The laser light was delivered through a silica optical fiber with a core diameter of 1,200 μm.

Optical Characteristics of Porcine Myocardium

The optical properties of porcine myocardium were obtained using Kubelka–Munk two-flux theory, in which the scattering and absorption coefficients can be directly expressed in terms of the measured reflectance, transmittance, and thickness of the tissue sample [19]. Extracted porcine ventricular myocardium was cut in approximately 1-mm thick slices and placed between 0.2-mm-thick glass slides. The diffused transmittance and reflectance of the tissue samples were measured at 663 nm by a spectrophotometer (UV-3600; Shimadzu Co., Kyoto, Japan), equipped with an integrating sphere. The Kubelka–Munk coefficients A_{KM} and S_{KM} are related to transport coefficients using the following relations [20]:

$$A_{KM} = 2\mu_a, \quad S_{KM} = \frac{1}{4}(3\mu_s' - \mu_a) \tag{1}$$

The absorption coefficient, μ_a, and reduced scattering coefficient, μ_s', of the porcine myocardium were calculated with the measured diffused reflectance and transmittance.

Photosensitizer Concentration in Plasma

The NPe6 concentration in plasma during the procedure was measured to obtain the decay curve of the plasma concentration with time. The photosensitizer concentration in plasma might have a proportional relation to that in tissue; NPe6 concentration in heart is reported to be about one-sixth of that in plasma [21]. Porcine blood samples were collected in evacuated tubes containing ethylenediamine tetra-acetic acid (EDTA) 5–60 minutes after the photosensitizer injection. The blood samples were centrifuged at 3,000 rpm for 10 minutes at 4°C. The optical absorption spectra of NPe6 in the plasma were measured in the wavelength range of 350–710 nm by the spectrophotometer. The obtained absorption peak area of the Q band was determined using the baseline method and converted into the NPe6 concentration by comparison with a calibration curve constructed previously using known photosensitizer concentrations.

Electrophysiological Study in the Acute Phase

To demonstrate the acute and transmural electrical conduction block with the photosensitization reaction, we designed an electrophysiological study using porcine atrial appendage. The porcine chest was surgically opened, and the left atrial appendage (1–3 mm thickness) was exposed through an incision in the lateral chest wall. With the heart beating, two plunge electrodes (electrodes A and B) were inserted onto the atrial appendage. Electrode A was used for electrical stimulation of the myocardium with stimulation conditions of 6.3 milliseconds pulse width, 3.0 Hz frequency, and 1.5 V amplitude. Electrode B was used to measure the propagated activation signal. The measured electrical signals were amplified by Bio Amplifier (PowerLab, ADInstruments, Hastings, UK) and recorded by a computer with a data acquisition program, Chart 4 (ADInstruments). NPe6 dissolved in physiological saline was injected intravenously at 10 mg/kg into the pigs (around 15 kg, $n = 2$). The laser irradiation via the optical fiber started 30 minutes after the injection. The optical fiber was not in direct contact with the myocardial surface; instead, it was fixed by hand using a spacer to keep a constant distance of about 18 mm between the fiber tip and myocardial surface. The red laser light beam, with a spot size of 7 mm at a power density of 5.2 W/cm^2 and a total energy density of 208 J/cm^2, was irradiated point by point to make about 35-mm irradiation line between the two electrodes so that the adjacent irradiated areas overlapped by about 30%. The conduction time from electrode A to B was measured immediately (within 1 minute) after each irradiation to assess the acute

myocardial electrical conduction block by the photosensitization reaction. If the transmural conduction block was obtained during the procedure as in the case with radiofrequency ablation, the conduction time might be prolonged depending on the irradiation length to wrap around the transmural conduction block line.

Histopathological Study in the Chronic Phase

The porcine chest was surgically opened, and the left atrial appendage was exposed as described before. NPe6, dissolved in physiological saline at 5 mg/kg, was injected intravenously into pigs weighing about 24 kg ($n = 2$). Fifteen minutes after the injection, the red laser light beam was irradiated through the optical fiber on the surface of the atrial appendage as described previously with a spot size of 3 mm, power density of 3.5 W/cm^2, and total energy density of 50 or 100 J/cm^2. During the irradiation, the temperature change on the tissue surface was measured with an infrared thermo-camera (Avio TVS-500; Nippon Avionics, Ltd, Tokyo, Japan). Two weeks after the procedure, the pigs were euthanized, and their hearts were extracted and subsequently fixed in 10% formalin. The fixed heart samples were sectioned, and the cross-sectional slices at the irradiated sites were used to determine the area affected by the photosensitization reaction. The irradiated site was identified by the anatomical features of the appendage. The tissue specimens were stained with standard staining for histological examination; hematoxylin and eosin (HE) to examine the extent of viable or nonviable cells and changes in cellular and nuclear morphology, or Azan to differentiate between the normal and affected areas replaced by fibrotic (scar) tissue.

RESULTS

Optical Properties of the Porcine Myocardium at 663 nm

The absorption coefficient (μ_a), reduced scattering coefficient (μ_s'), effective attenuation coefficient (μ_{eff}), and optical penetration depth (δ) of the porcine ventricular myocardium at 663 nm were obtained by Equation (1). μ_{eff} and δ were obtained from the following equation: $\mu_{eff} = \delta^{-1} = \sqrt{3\mu_a(\mu_a + \mu_s')}$. The obtained parameters of the porcine myocardium were as follows: $\mu_a = 0.35\,mm^{-1}$, $\mu_s' = 0.68\,mm^{-1}$, $\mu_{eff} = 1.0\,mm^{-1}$, and $\delta = 0.96\,mm^{-1}$. The obtained absorption and scattering coefficients at 663 nm were within the range of previously reported data: $0.1 < \mu_a < 0.6\ mm^{-1}$, $0.6 < \mu_s' < 1.4\ mm^{-1}$ in the wavelength range of 600–700 nm [22,23].

Decay of NPe6 Concentration in Porcine Plasma

The NPe6 concentration in plasma between 5 minutes and 1 hour after the administration of 5 or 10 mg/kg NPe6 to the pigs ($n = 2$) during the procedure was measured. The plasma concentration of NPe6 decreased with time, exhibiting kinetics similar to previously reported data [24]. Similar to that reported in humans, the observed decay curve of plasma concentration with time could be divided in two phases [17]: the measured elimination half-life was about 7 minutes in the initial rapid exponential decline (the first phase) and about 77 minutes in the subsequent slower exponential decline (the second phase). In this study, the drug–light interval was determined to be 15–30 minutes, during which the NPe6 concentration in plasma was about 10 μg/ml, decreasing relatively gently in the second exponential decline phase. Our preliminary studies demonstrated the photosensitization reaction-induced electrical conduction block with a plasma concentration of 8 μg/ml in extracted rat hearts [25].

Acute Electrical Conduction Block With the Photosensitization Reaction

To demonstrate the acute myocardial electrical conduction block as a result of the photosensitization reaction, the conduction time of the electrical signal from electrode A to B after each irradiation was assessed using the exposed porcine left atrial appendage *in vivo* from the acute phase study. Figure 1 shows a macroscopic photograph of the left atrial appendage extracted immediately after the procedure, indicating the electrode arrangements and irradiated site. Although there was uneven coloration on the tissue surface of the atrial appendage due to variations in tissue thickness, we found no obvious evidence of acute thermal coagulation or edema formation. Figure 2 shows the electrical potential waveforms at the measuring electrode B immediately after each irradiation. The conduction time of the electrical signal generated at the

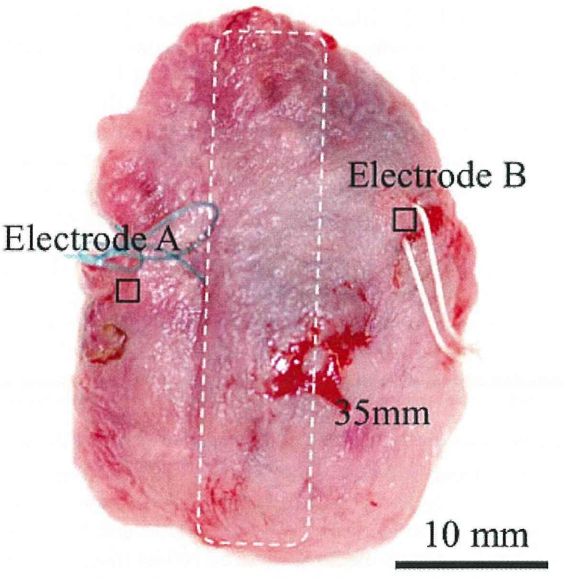

Fig. 1. A macroscopic photograph of a left atrial appendage extracted after the procedure. The extracted atrial appendage was washed with biological saline to remove blood. The area enclosed within the white dotted line shows the irradiated area. The length of the irradiated area is about 35 mm. The open squares indicate the sites of the stimulation and measurement electrodes in the myocardial tissue.

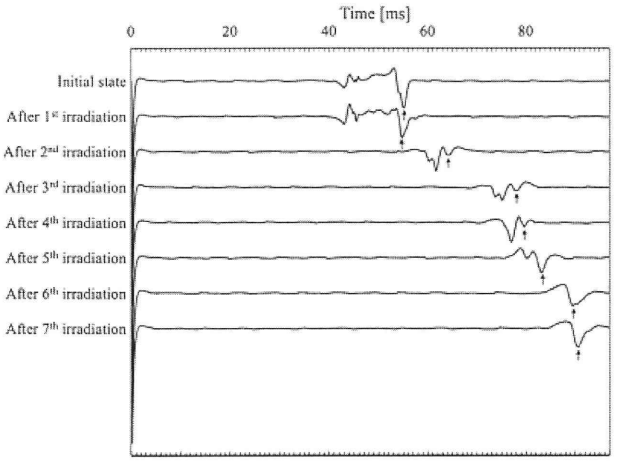

Fig. 2. The electrical potential signal recorded at electrode B in the initial state and after each irradiation. A shift in the electrical waveform indicates a conduction delay at electrode B as result of the photosensitization reaction. The black arrows indicate the time used to calculate the conduction time from stimulation to measurement at electrode B after each irradiation.

stimulated site and propagating to electrode B (t_{A-B}) was prolonged after each irradiation, indicating that the electrical response of the myocardium was obtained immediately (within 1 minute) after irradiation. The obtained values of t_{A-B} were 55.2 milliseconds at the initial state and 90.7 milliseconds after the sequence of the irradiations; a conduction delay of 35.5 milliseconds from the initial state was recorded.

Chronic Electrical Conduction Block as a Result of the Photosensitization Reaction

To demonstrate the permanent myocardial electrical conduction block as a result of the photosensitization reaction, chronic histopathological observations of the porcine left atrial appendage were examined *in vivo*. Figure 3 shows a macroscopic photograph of an extracted left atrial appendage fixed in formalin 2 weeks after the procedure. There were no obvious changes in tissue color on the surface of the irradiated area. Furthermore, there was no evidence of thermal damage in the irradiated area, which would be characterized by hemorrhage and edema surrounding coagulation necrosis. The measured temperature increase on the surface of the irradiated area during the irradiation was about 12.8°C. Figure 4 is a microscopic image of Azan- and HE-stained specimens at total energy densities of 50 J/cm^2, 2 weeks after the procedure. We found that the areas affected by the photosensitization reaction were demarcated and replaced transmurally with fibrosis tissue in the Azan-stained specimens (Fig. 4a). Neither myocardial wall rupture nor endocardial thrombi were observed. The maximum depths affected by the photosensitization reaction were >1.0 mm at a total energy density of 50 J/cm^2 and >1.3 mm at 100 J/cm^2.

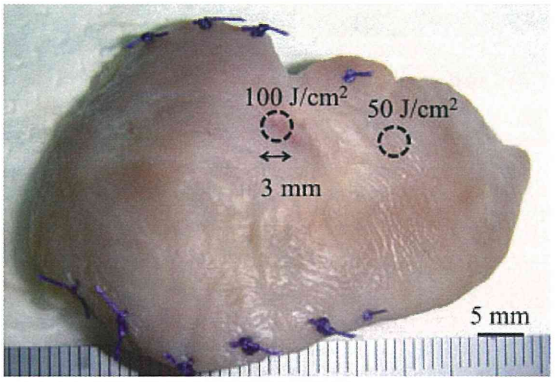

Fig. 3. A macroscopic photograph of a left atrial appendage fixed in formalin 2 weeks after the procedure. The dotted open circles indicate the irradiated sites.

Since the tissue thickness of the atrial appendage was around 1 mm in the irradiated area, the affected depth might exceed 1 mm under these irradiation conditions. There was almost no shrinkage in the affected area compared with the normal area, so that the reduction in size due to the scar shrinkage might be negligible. Microscopic observations of the HE-stained specimens indicate that the affected area exhibited nuclear shrinkage and loss of muscle striations (Fig. 4b) in comparison with the normal area (Fig. 4c). These tissue changes might induce a permanent electrical conduction block.

DISCUSSION

The estimated length of the shortest path to wrap around the irradiation line (Fig. 1) indicates that the change in the conduction pathway might be 22 mm. The conduction delay corresponding to the expected conduction pathway change is calculated to be 22–55 milliseconds with the reported conduction velocity in the mammalian atrial appendage of 0.4–1.0 m/second [26]. The measured conduction delay of 35.5 milliseconds is within the range of the above calculated value. These results suggest that the conduction delay is due to the change in the conduction pathway induced by transmural myocardial electrical conduction block obtained immediately after the photosensitization reaction. In the short drug–light interval condition, the photosensitizer might be distributed mainly in the blood and interstitial spaces of myocardium; it is reported that NPe6 might get into the interstitial spaces <20 minutes after the injection [27,28]. The photosensitization reaction with an interstitial space-distributed photosensitizer might induce immediate necrotic-like cell damage, which may be responsible for the acute myocardial electrical conduction block [25,29]. Our previous report indicates that the damage to ion channels and cell membranes induced by the photosensitization reaction might cause an influx of Ca^{2+}, rapid increase in the intracellular Ca^{2+} concentration, and eventually a necrotic cell response [29]. The acute myocardial electrical response to the photosensitization reaction

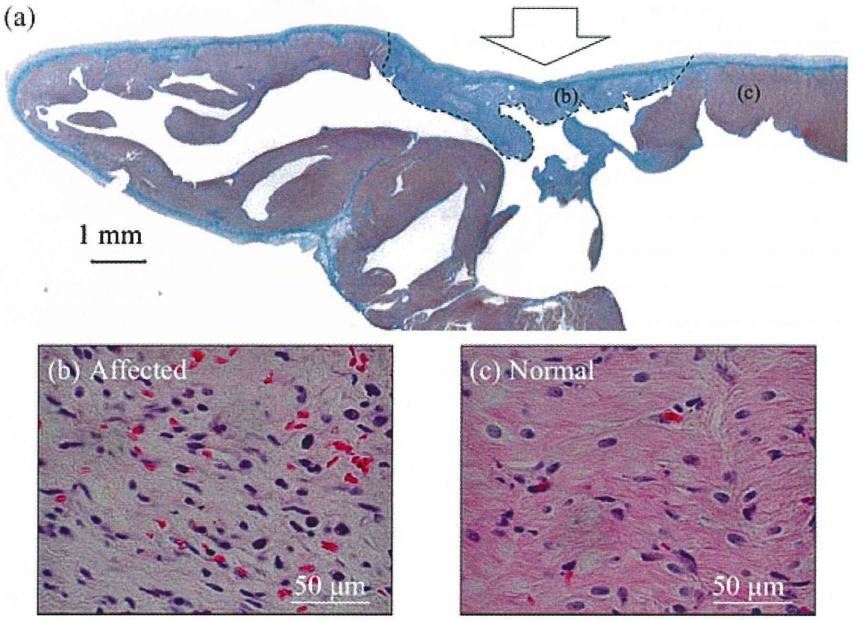

Fig. 4. **a**: An Azan-stained specimen of the irradiated area of a porcine left atrial appendage. The red laser light was irradiated from the direction of the arrow with a spot size of 3 mm, power density of 3.5 W/cm^2, and total energy density of 50 J/cm^2. The border between the affected and normal region was demarcated by the black dotted line. **b**,**c**: The HE-stained specimens of (b) the affected area and (c) the normal area indicated in (a).

was also demonstrated by the authors with exposed rat hearts *in vivo* [25].

The affected tissue depth by the photosensitization reaction obtained in the chronic histopathological study is reasonable on the basis of the measured optical penetration depth in the myocardium of 0.96 mm at 663 nm. As the condition of the photosensitization reaction is almost the same between the acute and chronic phase study, these results suggested that the acute electrical conduction block obtained in the electrophysiological evaluation might be kept in the chronic case. The observed tissue changes might be due to the oxidative process with the photosensitization reaction and not the thermal process, because the tissue temperature during the irradiation on the myocardial surface was <50°C for irradiation durations <30 seconds. It is reported that irreversible thermal damage in myocardium, including irreversible cellular electrophysiological changes and thermal denaturation is observed at temperatures exceeding 50°C for several minutes [30,31]. The temperature increase of the myocardium is rather small with the photosensitization reaction, compared to thermal ablation therapies in which the maximum temperature of the myocardial surface during the ablation is around 80°C [32,33]. The small temperature increase in the photosensitization reaction might be due to the low input power; the input power required to create a myocardial lesion with 2–3 mm in diameter and several millimeter deep may be <1 W for the photosensitization reaction, and is reported to be 10–30 W for laser ablation [7–9], and 20–50 W for radiofrequency ablation [32]. The energy consumption used for singlet oxygen generation in the photosensitization reaction with NPe6 is roughly estimated to be 1.9% of the total input energy under the experimental conditions, by considering (i) a molar absorption coefficient of NPe6, (ii) a quantum yield of singlet oxygen generation, and (iii) a NPe6 concentration in myocardium [18,21]. In contrast, almost all of the total input energy is used to generate heat in the thermal ablations. Therefore, the process of myocardial tissue damage with oxidative interaction in the photosensitization reaction is energy efficient. We think that catheterization application to cardiac ablation with the photosensitization reaction may be promising approach in non-thermal arrhythmia therapy, because temperature increase of the irradiated tissue might be suppressed by cooling effect of blood flow.

The electrophysiology and histology evaluation were conducted with healthy young pigs. Due to the rapid clearance of NPe6 from the body, large amount of the photosensitizer dose was needed in order to obtain optimal condition of photosensitizer concentration in plasma during the procedure, so that young light-weight pigs were used. In the case of human, the excretion rate of NPe6 is slower than that in animals; the elimination half-life of NPe6 is about 9 hours, so that the plasma concentration of the photosensitizer might be almost constant for several hours after the injection [17]. The myocardium of arrhythmia patients might have different structure and

function to the normal one; the optical properties and photosensitizer pharmacokinetics in the myocardium may change with the disease progression, such as collagen content of the myocardium. These factors need to be taken into account when determining the treatment protocol for clinical studies. In the measurement of the optical properties, we used ventricular tissue rather than atrial tissue. The measured optical properties of atrial ($n = 2$) and ventricular myocardium ($n = 16$) were almost the same, so that we showed the results with ventricular myocardium as the statistically collected value.

In conclusion, we demonstrated acute and chronic myocardial electrical conduction blocks as a result of the photosensitization reaction with NPe6 in the porcine left atrial appendage. The electrophysiological study indicated that the photosensitization reaction induced acute electrical conduction block according to the conduction delay of the electrical signal. The histopathological study showed that the photosensitization reaction induced transmural tissue scarring, indicating permanent electrical conduction block. These results indicate that a nonthermal catheter ablation using a photosensitization reaction could be applied in arrhythmia therapy.

ACKNOWLEDGMENTS

This study was partially supported by the Supporting Program for Creating University Ventures (#1904) of the Japan Science and Technology Agency and Research Fellowships of the Japan Society for the Promotion of Science for Young Scientists.

REFERENCES

1. Camm AJ, Kirchhof P, Lip GYH, Schotten U, Savelieva I, Ernst S, Van Gelder IC, Al-Attar N, Hindricks G, Prendergast B, Heidbuchel H, Alfieri O, Angelini A, Atar D, Colonna P, De Caterina R, De Sutter J, Goette A, Gorenek B, Heldal M, Hohloser SH, Kolh P, Heuzey JYL, Ponikowski P, Rutten FH. Guidelines for the management of atrial fibrillation. Eur Heart J 2010;31:2369–2429.
2. Nault I, Miyazaki S, Forclaz A, Wright M, Jadidi A, Jais P, Hocini M, Haissaguerre M. Drugs vs. ablation for the treatment of atrial fibrillation: The evidence supporting catheter ablation. Eur Heart J 2010;31:1046–1054.
3. Wazni OM, Marrouche NF, Martin DO, Verma A, Bhargava M, Saliba W, Bash D, Schweikert R, Brachmann J, Gunther J, Gutleben K, Pisano E, Potenza D, Fanelli R, Raviele A, Themistoclakis S, Rossillo A, Bonso A, Natale A. Radiofrequency ablation vs. antiarrhythmic drugs as first-line treatment of symptomatic atrial fibrillation. JAMA 2005;293: 2634–2640.
4. Cappato R, Calkins H, Chen SA, Davies W, Iesaka Y, Kalman J, Kim YH, Klein G, Natale A, Packer D, Skanes A, Ambrogi F, Biganzoli E. Updated worldwide survey on the methods, efficacy, and safety of catheter ablation for human atrial fibrillation. Circ Arrhythm Electrophysiol 2010;3:32–38.
5. Dagres N, Hindricks G, Kottkamp H, Sommer P, Gaspar T, Bode K, Arya A, Husser D, Rallidis LS, Kremastinos DTH, Piorkowski C. Complications of atrial fibrillation ablation in a high-volume center in 1,000 procedures: Still cause for concern. J Cardiovasc Electrophysiol 2009;20:1014–1019.
6. Cappato R, Calkins H, Chen SA, Davies W, Iesaka Y, Kalman J, Kim YH, Klein G, Packer D, Skanes A. Worldwide survey on the methods, efficacy, and safety of catheter ablation for human atrial fibrillation. Circulation 2005;111: 1100–1105.
7. Thomas SP, Guy DJR, Rees A, Collins L, Ross DL. Production of narrow but deep lesions suitable for ablation of atrial fibrillation using a saline-cooled narrow beam Nd:YAG laser catheter. Lasers Surg Med 2001;38:375–380.
8. Curtis AB, Mansour M, Fridel SE, Tomaru T, Barbeau GR, Normann SJ, Abela GS. Modification of atrioventricular conduction using a combined laser-electrode catheter. Pacing Clin Electrophysiol 1994;17:337–348.
9. Wagshall A, Abela GS, Maheshwari A, Gupta A, Bowden R, Huang SKS. A novel catheter design for laser photocoagulation of the myocardium to ablate ventricular tachycardia. J Interv Card Electrophysiol 2002;7:13–22.
10. Dougherty TJ, Gomer CJ, Henderson BW, Jori G, Kessel D, Korbelik M, Moan J, Peng Q. Photodynamic therapy. J Natl Cancer Inst 1998;90:889–905.
11. Schuitmaker JJ, Baas P, van Leengoed HL, van der Meulen FW, Star WM, van Zandwijk N. Photodynamic therapy: A promising new modality for the treatment of cancer. J Photochem Photobiol B 1996;34:3–12.
12. Dougherty TJ. Photodynamic therapy. Photochem Photobiol 1993;58:895–900.
13. Moore JV, West CML, Whitehurst C. The biology of photodynamic therapy. Phys Med Biol 1997;42:913–935.
14. Oleinick NL, Morris RL, Belichenko I. The role of apoptosis in response to photodynamic therapy: What, where, why, and how. Photochem Photobiol Sci 2002;1:1–21.
15. Buytaert E, Dewaele M, Agostinis P. Molecular effectors of multiple cell death pathways initiated by photodynamic therapy. Biochim Biophys Acta 2007;1776:86–107.
16. Kato H, Furukawa K, Sato M, Okunaka T, Kusunoki Y, Kawahara M, Fukuoka M, Miyazawa T, Yana T, Matsui K, Shiraishi T, Horinouchi H. Phase II clinical study of photodynamic therapy using mono-L-aspartyl chlorin e6 and diode laser for early superficial squamous cell carcinoma of the lung. Lung Cancer 2003;42:103–111.
17. Kessel D. Pharmacokinetics of N-aspartyl chlorin e6 in cancer patients. J Photochem Photobiol B 1997;39:81–83.
18. Spikes JD, Bommer JC. Photosensitizing properties of mono-L-aspartyl chlorin e6 (NPe6): A candidate sensitizer for the photodynamic therapy of tumors. J Photochem Photobiol B 1993;17:135–143.
19. Cheong WF, Prahl SA, Welch AJ. A review of the optical properties of biological tissues. IEEE J Quantum Electron 1990;26:2166–2185.
20. Star WM, Marijnissen JPA, van Gernert MJC. Light dosimetry in optical phantoms and in tissues: I. Multiple flux and transport theory. Phys Med Biol 1988;33:437–454.
21. Gomer CJ, Ferrario A. Tissue distribution and photosensitizing properties of mono-L-aspartyl chlorin e6 in a mouse tumor model. Cancer Res 1990;50:3985–3990.
22. Pickering JW, Bosman S, Posthumus P, Blokland P, Beek JF, van Gemert MJ. Changes in the optical properties (at 632.8nm) of slowly heated myocardium. Appl Opt 1993;32: 367–371.
23. Swartling J, Pålsson S, Platonov P, Olsson SB, Andersson-Engels S. Changes in tissue optical properties due to radiofrequency ablation of myocardium. Med Biol Eng Comput 2003;41:403–409.
24. Kondo K, Miyoshi T, Fujino H, Takizawa H, Imai S, Kobayashi N, Kenzaki K, Sakiyama S, Tangoku A. Photodynamic therapy using a second generation photosensitizer, Talaporfin. Photodiagnosis Photodyn Ther 2007;4:269–274.
25. Ito A, Hosokawa S, Miyoshi S, Soejima K, Ogawa S, Arai T. The myocardial electrical blockade induced by photosensitization reaction. IEEE Trans Biomed Eng 2010;57: 488–495.
26. Draper MH, Mya-TU M. A comparison of the conduction velocity in cardiac tissues of various mammals. Q J Exp Physiol Cogn Med Sci 1959;44:91–109.
27. Mitra S, Foster TH. In vivo confocal fluorescence imaging of the intratumor distribution of the photosensitizer mono-L-aspartylchlorin-e6. Neoplasia 2008;10:429–438.
28. Pegaz B, Debefve E, Borle F, Ballini JP, Wagnieres G, Spaniol S, Albrecht V, Scheglmann D, Nifantiev NE, van den Bergh H, Konan YN. Preclinical evaluation of a novel

water-soluble chlorin e6 derivative (BLC 1010) as photosensitizer for the closure of the neovessels. Photochem Photobiol 2005;81:1505–1510.
29. Ito A, Kimura T, Miyoshi S, Ogawa S, Arai T. Photosensitization reaction-induced acute electrophysiological cell response of rat myocardial cells in short loading periods of talaporfin sodium or porfimer sodium. Photochem Photobiol 2011;87:199–207.
30. Haines DE. The biophysics of radiofrequency catheter ablation in the heart: The importance of temperature monitoring. Pacing Clin Electrophysiol 1993;16:586–591.
31. Whayne JG, Nath S, Haines DE. Microwave catheter ablation of myocardium in vitro. Assessment of the characteristics of tissue heating and injury. Circulation 1994;89:2390–2395.
32. Wittkampf FH, Nakagawa H. RF catheter ablation: Lessons on lesions. Pacing Clin Electrophysiol 2006;29:1285–1297.
33. Matsudaira K, Nakagawa H, Wittkampf FH, Yamanashi WS, Imai S, Pitha JV, Lazzara R, Jackman WM. High incidence of thrombus formation without impedance rise during radiofrequency ablation using electrode temperature control. Pacing Clin Electrophysiol 2003;26:1227–1237.

J Artif Organs (2011) 14:171–177
DOI 10.1007/s10047-011-0578-4

MINIREVIEW

Tissue engineering and cell-based therapy toward integrated strategy with artificial organs

Satoshi Gojo · Masashi Toyoda · Akihiro Umezawa

Received: 9 May 2011 / Accepted: 19 May 2011 / Published online: 10 June 2011

Abstract Research in order that artificial organs can supplement or completely replace the functions of impaired or damaged tissues and internal organs has been underway for many years. The recent clinical development of implantable left ventricular assist devices has revolutionized the treatment of patients with heart failure. The emerging field of regenerative medicine, which uses human cells and tissues to regenerate internal organs, is now advancing from basic and clinical research to clinical application. In this review, we focus on the novel biomaterials, i.e., fusion protein, and approaches such as three-dimensional and whole-organ tissue engineering. We also compare induced pluripotent stem cells, directly reprogrammed cardiomyocytes, and somatic stem cells for cell source of future cell-based therapy. Integrated strategy of artificial organ and tissue engineering/regenerative medicine should give rise to a new era of medical treatment to organ failure.

This article is a translation of an article that appeared in *The Japanese Journal of Artificial Organs* 2010;39:202–207.

S. Gojo (✉)
Department of Therapeutic Strategy for Heart Failure,
Graduate School of Medicine, University of Tokyo,
7-3-1 Hongo, Bunkyo, Tokyo 113-8655, Japan
e-mail: satoshigojo-tky@umin.ac.jp

M. Toyoda
Research Team for Vascular Medicine,
Tokyo Metropolitan Institute of Gerontology, Tokyo, Japan

A. Umezawa (✉)
Department of Reproductive Biology,
National Institute for Child Health and Development,
2-10-1, Okura, Setagaya, Tokyo 157-8535, Japan
e-mail: umezawa@1985.jukuin.keio.ac.jp

Keywords Biofabrication · Stem cell · Reprogramming · Direct conversion · Clinical trial

Introduction

The human body is made up of approximately 60 trillion cells but can be traced back to one fertilized egg created by the union of an ovum and a sperm. The fertilized egg divides repeatedly, creating various cells that coordinate with each other to form all the different tissues and organs, ultimately leading to the formation of a complete individual. Whereas the human genome has been almost completely decoded and the genes involved in various mechanisms of the body are becoming known, many parts of this epic developmental process remain unclear. However, because these developmental mechanisms are closely related to the homeostatic maintenance and the regenerative mechanisms of organs and tissues, the field of regenerative medicine, which aims to use these mechanisms to treat diseases, is expanding rapidly.

Tissue engineering

Fusion protein

Biological tissue is composed not only of cells but also of a surrounding environment that is crucial in maintaining cell function in vivo and in homeostasis. Most importantly, the extracellular matrix is known to have dynamic and functional roles, such as providing a scaffold for cell adhesion (basement membrane and fibronectins) as well as maintaining and providing growth factors (heparan sulfate). Technological development with respect to manipulating

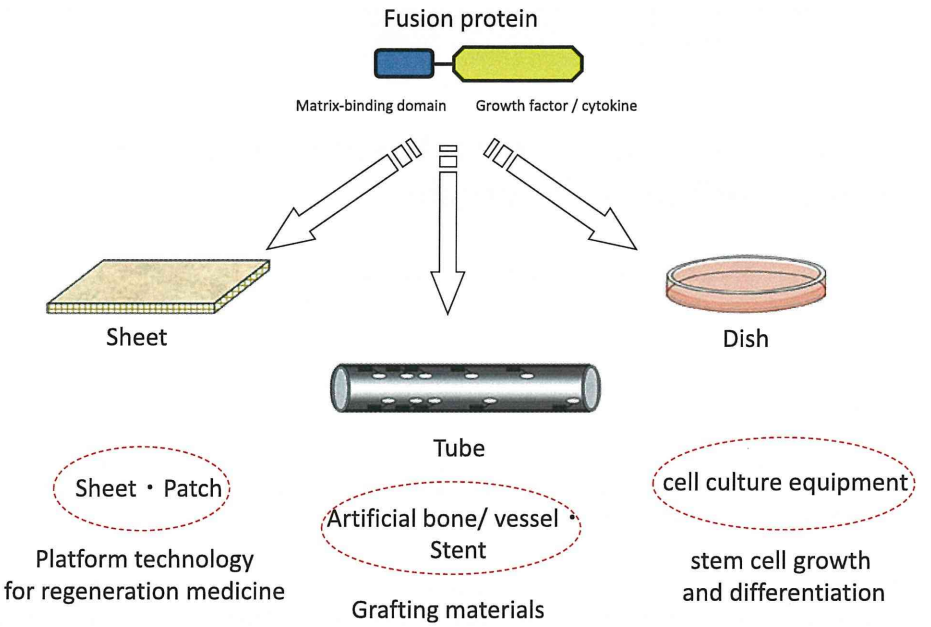

Fig. 1 Tissue engineering for regenerative medicine

this extracellular matrix in order to control tissues and cells, and its subsequent application in regenerative medicine, is underway. For example, studies have revealed that a variety of growth factors play important roles in wound healing, and some of these growth factors are in clinical use. However, the short-term effects of these growth factors pose some limitations on their use. An example is provided by fibrin, which is released in the wounded area when tissue damage occurs. An increasing amount of research is being conducted on the use of fibrin as a material for tissue regeneration. If a protein produced by the fusion of a fibrin-binding domain (FBD) to epidermal growth factor (EGF) is added to an epidermal wound-model culture system, binding of the growth factor to the fibrin released from the wound leads to healing by stimulating growth in the surrounding cells [1]. This phenomenon presumably occurs not because of the independent function of the growth factor, but because the growth factor stabilizes after binding to fibrin, and the FBD–EGF complex causes continuous cell stimulation. This suggests that the process of altering the combination of extracellular matrix and growth factors can be of therapeutic value in a variety of conditions. Another example can be considered with respect to vascular grafts. The development of small-caliber vascular grafts, such as those used to treat coronary artery disease, has slowed down because these grafts tend to fail at an early stage owing to thrombotic occlusion. To prevent this, prompt graft endothelialization and prevention of blood clot adherence is necessary. The use of a protein produced by fusion of the collagen-binding domain (CBD)—which binds collagen (a component of the extracellular matrix)—to hepatocyte growth factor (HGF) has been considered in such cases, and it has been shown that this complex (CBD–HGF) effectively promotes growth of endothelial cells [2]. Furthermore, this type of fusion protein could be placed onto a biodegradable sheet of extracellular matrix and affixed to the wounded area, where it may stimulate vascular cell growth. This has the potential for a wide application in medicine (Fig. 1).

Three-dimensional tissue engineering

A substantial amount of tissue engineering research has been performed on the three-piece that are cell, growth factors, and scaffolds. There are, however, various limitations to using scaffolds. First, cells tend to be distributed over the surface of the scaffold, thus making it difficult to form a solid tissue. Second, a 3D array and structure cannot be controlled when multiple cell types are used. Third, the concentration gradient of growth factors cannot be controlled. Fourth, there are certain limitations to the process of creating the vasa vasorum by tissue engineering techniques. In recent years, the concept of the scaffold has been put aside, and attempts to construct 3D tissue with cells and growth factors are now frequently reported. This method is generally called biofabrication [3], and the techniques of bioprinting [4] and organ printing [5] also fit into this category. In addition, although 3D structures using inkjet printer technology have already appeared as rapid prototyping, a 3D printer with an inkjet nozzle from which

droplets with a volume identical to that of cells are embossed, and which can be operated in a sterile environment, has been developed [6]. This could make the construction of 3D tissues possible [7]. Biorapid prototyping, a method in which many cellular spheres are used together with arbitrary structures to create 3D tissue, has also been reported [8]. This is expected to be an extremely promising methodology despite many issues, such as those related to cell solvents.

Cell sheets

Of all the recently developed tissue engineering techniques, practical application of cell sheets has advanced the most. This technology is based on the properties of a temperature-responsive polymer, poly(*N*-isopropylacrylamide). Culture dishes coated with this material are hydrophobic at 37°C and hydrophilic <32°C. When cells are cultured to confluence, they can be recovered as a sheet without enzymatic digestion [9]. This technique has been made available from Japan for worldwide application in the development of regenerative medicine-related products [10]. It was reported that stratification, which was initially limited to a few layers, could evolve to include many layers with neovascularization. So far, cell sheets have been made that consist of myoblasts [11], mesenchymal stem cells [12], cardiac progenitor cells [13], and a mixture of fibroblasts and endothelial progenitors [14]. Osaka University is coordinating a clinical trial using autologous myoblast sheets in patients carrying a left ventricular assist device (LVAD) with the aim of providing a bridge to recovery. In France, a clinical trial using epithelial cell sheets for corneal regeneration is being conducted by a venture company.

Whole-organ tissue engineering

The technology of perfusion decellularization of organs is a unique method of tissue production using scaffolds that has been reported in recent years. Intracellular structures can be completely eliminated by perfusing the heart using a Langendorff coronary perfusion apparatus for more than 12 h with the surfactant sodium dodecyl sulfate. It has also been reported that components of the extracellular matrix, including collagen type I/III, laminin, and fibronectin, can be preserved without disturbing their array structure; furthermore, the structure of valves and basal membrane of the epicardial vessels are not affected [15]. A heartbeat, albeit faint, has been achieved using this technique. The feasibility of whole-organ decellularization has been demonstrated in the pig heart [16] and rat liver [17]. Although the process of cellularization has its flaws, it is a creative initiative that holds promise for future developments.

Regenerative medicine

Induced pluripotent stem cells (iPSC)

The term regenerative medicine was introduced in 2000. Clinical applications have increased greatly since then, beginning with research on human embryonic stem cells (ESC) and confirmation of the plasticity of somatic stem cells. Amid frustration that human ESC could not be applicable not only to medicine, but also in biological research, the phenomenon of initialization via nuclear transplantation has been achieved in an elaborately planned experiment with four gene transfers. Now, these cells, called induced pluripotent stem cells (iPSC), certainly appear to be a major topic in regenerative medicine. Basic research into the clinical application of iPSC demonstrated the successful treatment of model mice for Parkinson's disease [18], sickle cell anemia [19], and hemophilia [20] with mouse iPSC. These reports indicate the same scheme could be applicable to human diseases. However, problems in iPSC application include the development of teratomas from undifferentiated cells, carcinomas due to gene transfer, and infection with xenogeneic materials used in cell cultures. These problems have attracted the interest of a large number of researchers, and many proposals for solutions to them have been reported (Fig. 2).

Teratoma formation in mice can reportedly be prevented by eliminating stage-specific embryonic antigen-1-positive cells [18]. If the target of interest is the heart, enrichment with mitochondria could prevent teratoma formation [21]. Of the four genes transferred during iPSC initialization, which are considered to be reprogramming genes, it was feared that the existence of c-Myc, in particular, which is an oncogene, would lead to cancer; carcinogenesis through c-Myc reactivation was actually observed in vivo. In addition, because the basic protocol uses a retrovirus as the vector for gene transfer, the possibility of carcinogenesis after its insertion into a genome is a problem. It was subsequently reported that just three factors (excluding c-Myc) induced iPSC, albeit at a low frequency [22]. However, recently, induction of iPSC with RNA [23] and proteins [24] of reprogramming factors has been reported in an attempt to circumvent carcinogenesis because of the methodology. Of the four factors, Sox2 and c-Myc could be replaced with transforming growth factor-α receptor antagonists [25], the nuclear acceptor Esrrb could be replaced with Klf4 [26], and Oct4 could be replaced with nuclear acceptor Nr5a2 [27].

Currently, xenogeneic materials are used in various processes in standard ESC/iPSC culture (Fig. 3). Feeder cells are used to maintain the undifferentiated state of both ESC and iPSC; usually, mouse embryonic fibroblasts (MEF) treated with mitomycin C to arrest their growth are

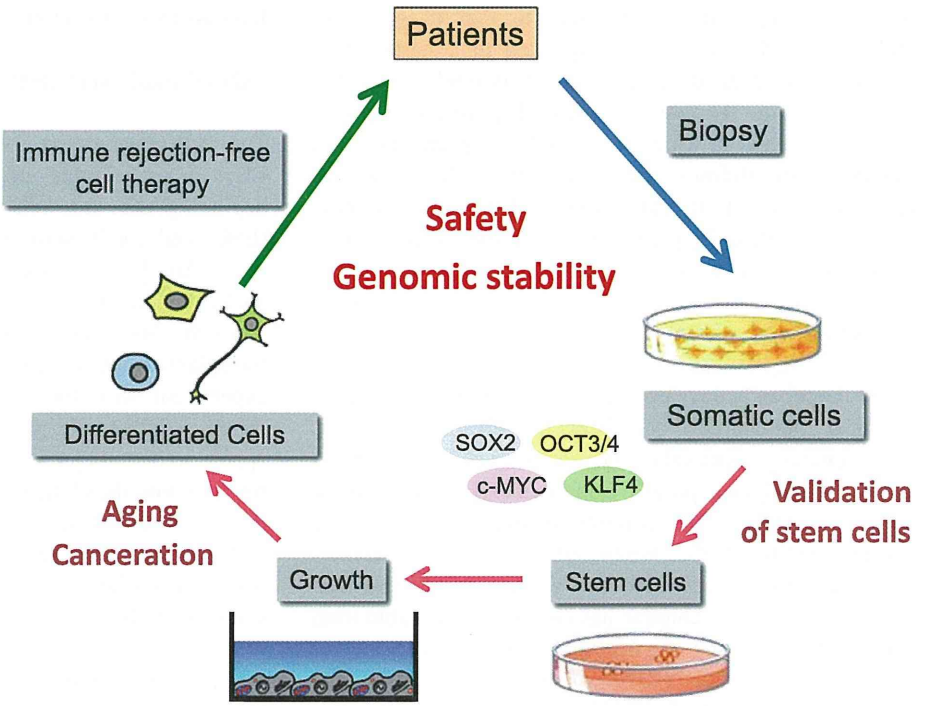

Fig. 2 Order-made stem cell therapy

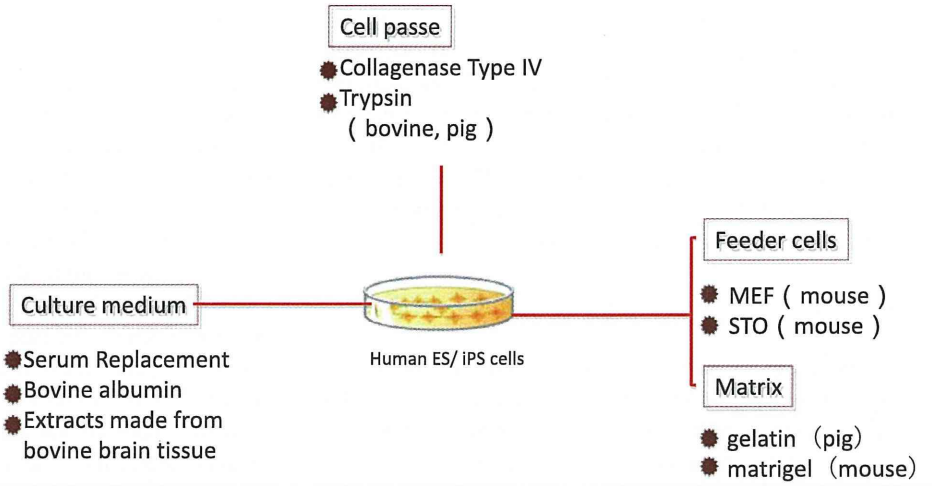

Fig. 3 Xenogeneic factors and materials in human embryonic stem cell/induced pluripotent stem cell (ESC/iPSC) culture

used as feeder cells. It was feared that if these xenogeneic cells were used in clinical situations, contamination with xenogeneic cells may lead to infection. This did, in fact, occur: the presence of non-human-derived Neu5Gc was confirmed on the cell surface of human ESC cultured onto MEF. Many individuals possess antibodies for this antigen, and an immune reaction can be provoked in these individuals [28]. In order to avoid xenogeneic contamination, coating cell culture dishes with fully synthetic compounds and the chemical defined-culture medium has been reported from several institutes. A 3D porous natural polymer scaffold consisting of chitosan and alginate was able to sustain human ESC self-renewal [29]. Recombinant vitronectin also supported cultivation of three human ESC under feeder-free conditions [30]. Moreover, suspension culture of human ESC and iPSC in chemically defined media supplied a scalable number of cells [31]. However, the ability of xeno-free protocols to maintain the self-renewal ability and pluripotency of human ESC or iPSC remains questionable. On the other hand, autologous

fibroblasts could be used as feeder cells in the culture of human iPSC [32].

Almost the entire process of reprogramming in iPSC remains poorly understood. It is still unclear whether iPSC reprogramming is equal to nuclear transplantation, which showed that the somatic nucleus reacquired totipotency. The following factors imply that multiple processes exist in reprogramming: the expression of stem cell-related genes differs between iPSC clones [33], and "memories" of the parent cells remain. It has been reported that trichostatin A, a histone deacetylase inhibitor, is a factor that promotes this phenomenon [34]. The necessity of using it under strictly controlled temporal and quantitative requirements indicates the preciseness of its mechanism.

Direct conversion to differentiated cells

The phenomenon termed direct conversion to differentiated cells is a novel occurrence recently reported to occur in several organs. Although many researchers have searched for the master gene, such as MyoD, that can induce formation of skeletal muscle cells from fibroblasts, no such gene has been discovered. However, because the use of four genes allows the differentiated cell to have pluripotency, transformation with one batch of gene transfer is been investigated. A first report described successful differentiation of pancreatic exocrine cells into insulin-secreting beta-like cells by the transfer of three genes (Ngn3/Pdx1/MafA) [35]. Another report documented successful induction of cells expressing myocardial cell structural proteins through the transfer of Gata4/Tbx5/Baf60c into mouse mesodermal cells [36]. According to later reports, functional neurons can be induced by transferring Asc11/Brn2/Myt11 into fibroblasts [37], and myocardial cells can be induced by transferring Gata4/Tbx5/Mef2c into fibroblasts [38]. Thus far, the possibility that these cells only caused specific gene expression that exists in the lower area of transgenes cannot be denied. Functional and quantitative assessments of induced cells produced by direct reprogramming are required to determine their application in the clinical setting.

Somatic stem cells

It was long believed that cardiomyocytes were in a state of terminal differentiation in adults and that the heart cannot heal itself or restore its homeostatic functions. These properties led researchers in cardiac regeneration to increased interest in somatic stem cells, including bone-marrow-derived stem/progenitor cells, mesenchymal stem cells, and adipose-derived stem cells. Because cells derived from fetal-related tissue (including the amnion, umbilical cord, and placenta) contain a multipotent population that shows plasticity, many organizations, institutes, and companies run banking systems for these cells. Transplantation of amniocytes caused cardiac regeneration in myocardial infarction in rats [39]. On the other hand, other researchers have continually asserted the heart has regenerative properties. Recently, clear evidence that cardiomyocytes can be reborn in the adult heart was reported. This evidence was based on cardiomyocyte age estimation by measuring carbon-14, which was generated by nuclear weapons testing during the Cold War [40]. The impetus for the expansion of this field of study was the reporting of a method that was apparently based on embryonic bodies [41]: by forming a sphere with cardiac-tissue-derived cells, a group of nearly undifferentiated cells could be enriched. Subsequently, several groups reported that stem cells and precursor cells exist in the heart. Several profiles were reported for these cells, including c-kit (+) [42], sca-1 (+) [43], and side population cells [44]. Whether this means that we are observing the process of differentiation as it develops or that multiple stem cell systems exist is an issue that needs to be addressed. Matsubara et al. [45], who reported that murine sca-1 (+) cells could be cardiac stem cells (CSC), performed a detailed preclinical study in pigs to treat ischemic heart disease [46] and are directing the world's first clinical trial using CSC. This clinical trial targets patients with severe chronic ischemic heart failure whose left ventricular ejection fraction is <35%. The method involves intramuscular injection of CSC during coronary artery bypass grafting. The injected stem cells are isolated from cardiac tissue collected during a previous biopsy from the right ventricular septal region. During cell culture, recombinant basic fibroblast growth factor (bFGF) is used rather than xenogeneic materials, and blood serum is obtained from autologous blood. The cells are injected through the epicardium, and the injection sites are covered with a basic sustained-release gelatin sheet of bFGF. Patients are not randomized, and six cases are scheduled for an open-label phase I/IIa clinical trial, with a planned 1-year follow-up study. It is assumed that after this trial, cases will accumulate in multifacility clinical studies and that this method will develop into a highly advanced medical technology.

Chemical pharmacology is faced with difficulty finding new classes of drugs despite increasing budgets. Cells and tissues, therefore, are likely to become important medical treatments. Moreover, integrated therapy of ventricular assist device (VAD) and regenerative medicine should have great potential to treat severe heart failure (Fig. 4). Although implantable VADs are being used with excellent prognosis, many issues remain; for example, right ventricular failure, infection, thrombosis, and device mechanical failure. A market report on VAD anticipates that the "bridge to recovery (BTR)" strategy will constitute more

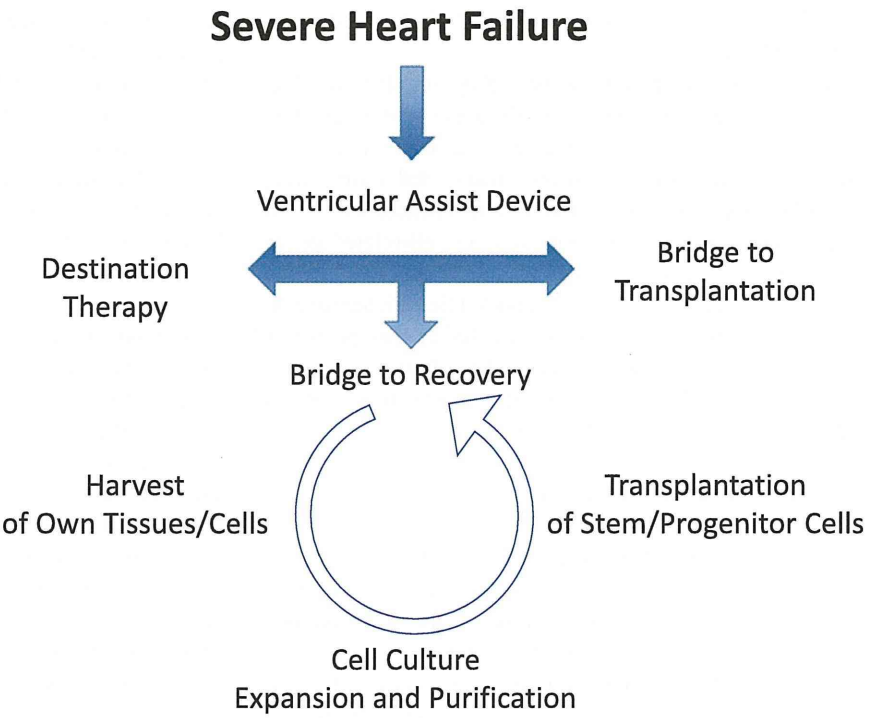

Fig. 4 Integrated strategy to heart failure

than half of future VAD therapy. The emerging field of regenerative medicine will surely accelerate the trend to BTR therapy.

References

1. Kitajima T, Sakuragi M, Hasuda H, Ozu T, Ito Y. A chimeric epidermal growth factor with fibrin affinity promotes repair of injured keratinocyte sheets. Acta Biomater. 2009;5:2623–32.
2. Ohkawara N, Ueda H, Shinozaki S, Kitajima T, Ito Y, Asaoka H, Kawakami A, Kaneko E, Shimokado K. Hepatocyte growth factor fusion protein having collagen-binding activity (CBD-HGF) accelerates re-endothelialization and intimal hyperplasia in balloon-injured rat carotid artery. J Atheroscler Thromb. 2007;14:185–91.
3. Mironov V, Trusk T, Kasyanov V, Little S, Swaja R, Markwald R. Biofabrication: a 21st century manufacturing paradigm. Biofabrication. 2009;1:022001.
4. Jakab K, Norotte C, Marga F, Murphy K, Vunjak-Novakovic G, Forgacs G. Tissue engineering by self-assembly and bio-printing of living cells. Biofabrication. 2010;2:022001.
5. Visconti RP, Kasyanov V, Gentile C, Zhang J, Markwald RR, Mironov V. Towards organ printing: engineering an intra-organ branched vascular tree. Expert Opin Biol Ther. 2010;10:409–20.
6. Nishiyama Y, Nakamura M, Henmi C, Yamaguchi K, Mochizuki S, Nakagawa H, Takiura K. Development of a three-dimensional bioprinter: construction of cell supporting structures using hydrogel and state-of-the-art inkjet technology. J Biomech Eng. 2009;131:035001.
7. Norotte C, Marga FS, Niklason LE, Forgacs G. Scaffold-free vascular tissue engineering using bioprinting. Biomaterials. 2009;30:5910–7.
8. Iwami K, Noda T, Ishida K, Morishima K, Nakamura M, Umeda N. Bio rapid prototyping by extruding/aspirating/refilling thermoreversible hydrogel. Biofabrication. 2010;2:014108.
9. Shimizu T, Yamato M, Kikuchi A, Okano T. Two-dimensional manipulation of cardiac myocyte sheets utilizing temperature-responsive culture dishes augments the pulsatile amplitude. Tissue Eng. 2001;7:141–51.
10. Shimizu T, Sekine H, Yamato M, Okano T. Cell sheet-based myocardial tissue engineering: new hope for damaged heart rescue. Curr Pharm Des. 2009;15:2807–14.
11. Miyagawa S, Saito A, Sakaguchi T, Yoshikawa Y, Yamauchi T, Imanishi Y, Kawaguchi N, Teramoto N, Matsuura N, Iida H, Shimizu T, Okano T, Sawa Y. Impaired myocardium regeneration with skeletal cell sheets—a preclinical trial for tissue-engineered regeneration therapy. Transplantation. 2010;90:364–72.
12. Hida N, Nishiyama N, Miyoshi S, Kira S, Segawa K, Uyama T, Mori T, Miyado K, Ikegami Y, Cui C, Kiyono T, Kyo S, Shimizu T, Okano T, Sakamoto M, Ogawa S, Umezawa A. Novel cardiac precursor-like cells from human menstrual blood-derived mesenchymal cells. Stem Cells. 2008;26:1695–704.
13. Fedak PW. Cardiac progenitor cell sheet regenerates myocardium and renews hope for translation. Cardiovasc Res. 2010;87:8–9.
14. Kobayashi H, Shimizu T, Yamato M, Tono K, Masuda H, Asahara T, Kasanuki H, Okano T. Fibroblast sheets co-cultured with endothelial progenitor cells improve cardiac function of infarcted hearts. J Artif Organs. 2008;11:141–7.
15. Ott HC, Matthiesen TS, Goh SK, Black LD, Kren SM, Netoff TI, Taylor DA. Perfusion-decellularized matrix: using nature's platform to engineer a bioartificial heart. Nat Med. 2008;14:213–21.
16. Wainwright JM, Czajka CA, Patel UB, Freytes DO, Tobita K, Gilbert TW, Badylak SF. Preparation of cardiac extracellular matrix from an intact porcine heart. Tissue Eng Part C Methods. 2010;16:525–32.
17. Soto-Gutierrez A, Zhang L, Medberry C, Fukumitsu K, Faulk D, Jiang H, Reing J, Gramignoli R, Komori J, Ross M, Nagaya M, Lagasse E, Stolz D, Strom SC, Fox IJ, Badylak SF.

A Whole-organ regenerative medicine approach for liver replacement. Tissue Eng Part C Methods 2011.
18. Wernig M, Zhao JP, Pruszak J, Hedlund E, Fu D, Soldner F, Broccoli V, Constantine-Paton M, Isacson O, Jaenisch R. Neurons derived from reprogrammed fibroblasts functionally integrate into the fetal brain and improve symptoms of rats with Parkinson's disease. Proc Natl Acad Sci USA. 2008;105:5856–61.
19. Hanna J, Wernig M, Markoulaki S, Sun CW, Meissner A, Cassady JP, Beard C, Brambrink T, Wu LC, Townes TM, Jaenisch R. Treatment of sickle cell anemia mouse model with iPS cells generated from autologous skin. Science. 2007;318:1920–3.
20. Xu D, Alipio Z, Fink LM, Adcock DM, Yang J, Ward DC, Ma Y. Phenotypic correction of murine hemophilia A using an iPS cell-based therapy. Proc Natl Acad Sci USA. 2009;106:808–13.
21. Hattori F, Chen H, Yamashita H, Tohyama S, Satoh YS, Yuasa S, Li W, Yamakawa H, Tanaka T, Onitsuka T, Shimoji K, Ohno Y, Egashira T, Kaneda R, Murata M, Hidaka K, Morisaki T, Sasaki E, Suzuki T, Sano M, Makino S, Oikawa S, Fukuda K. Nongenetic method for purifying stem cell-derived cardiomyocytes. Nat Methods. 2010;7:61–6.
22. Nakagawa M, Koyanagi M, Tanabe K, Takahashi K, Ichisaka T, Aoi T, Okita K, Mochiduki Y, Takizawa N, Yamanaka S. Generation of induced pluripotent stem cells without Myc from mouse and human fibroblasts. Nat Biotechnol. 2008;26:101–6.
23. Warren L, Manos PD, Ahfeldt T, Loh YH, Li H, Lau F, Ebina W, Mandal PK, Smith ZD, Meissner A, Daley GQ, Brack AS, Collins JJ, Cowan C, Schlaeger TM, Rossi DJ. Highly efficient reprogramming to pluripotency and directed differentiation of human cells with synthetic modified mRNA. Cell Stem Cell. 2010;7:618–30.
24. Kim D, Kim CH, Moon JI, Chung YG, Chang MY, Han BS, Ko S, Yang E, Cha KY, Lanza R, Kim KS. Generation of human induced pluripotent stem cells by direct delivery of reprogramming proteins. Cell Stem Cell. 2009;4:472–6.
25. Maherali N, Hochedlinger K. Tgfbeta signal inhibition cooperates in the induction of iPSCs and replaces Sox2 and cMyc. Curr Biol. 2009;19:1718–23.
26. Feng B, Jiang J, Kraus P, Ng JH, Heng JC, Chan YS, Yaw LP, Zhang W, Loh YH, Han J, Vega VB, Cacheux-Rataboul V, Lim B, Lufkin T, Ng HH. Reprogramming of fibroblasts into induced pluripotent stem cells with orphan nuclear receptor Esrrb. Nat Cell Biol. 2009;11:197–203.
27. Heng JC, Feng B, Han J, Jiang J, Kraus P, Ng JH, Orlov YL, Huss M, Yang L, Lufkin T, Lim B, Ng HH. The nuclear receptor Nr5a2 can replace Oct4 in the reprogramming of murine somatic cells to pluripotent cells. Cell Stem Cell. 2010;6:167–74.
28. Martin MJ, Muotri A, Gage F, Varki A. Human embryonic stem cells express an immunogenic nonhuman sialic acid. Nat Med. 2005;11:228–32.
29. Li Z, Leung M, Hopper R, Ellenbogen R, Zhang M. Feeder-free self-renewal of human embryonic stem cells in 3D porous natural polymer scaffolds. Biomaterials. 2010;31:404–12.
30. Braam SR, Zeinstra L, Litjens S, Ward-van Oostwaard D, van den BS, van Laake L, Lebrin F, Kats P, Hochstenbach R, Passier R, Sonnenberg A, Mummery CL, et al. Recombinant vitronectin is a functionally defined substrate that supports human embryonic stem cell self-renewal via alphavbeta5 integrin. Stem Cells. 2008;26:2257–65.
31. Olmer R, Haase A, Merkert S, Cui W, Palecek J, Ran C, Kirschning A, Scheper T, Glage S, Miller K, Curnow EC, Hayes ES, Martin U. Long term expansion of undifferentiated human iPS and ES cells in suspension culture using a defined medium. Stem Cell Res. 2010;5:51–64.
32. Takahashi K, Narita M, Yokura M, Ichisaka T, Yamanaka S. Human induced pluripotent stem cells on autologous feeders. PLoS One. 2009;4:e8067.
33. Miura K, Okada Y, Aoi T, Okada A, Takahashi K, Okita K, Nakagawa M, Koyanagi M, Tanabe K, Ohnuki M, Ogawa D, Ikeda E, Okano H, Yamanaka S. Variation in the safety of induced pluripotent stem cell lines. Nat Biotechnol. 2009;27:743–5.
34. Kishigami S, Van Thuan N, Hikichi T, Ohta H, Wakayama S, Mizutani E, Wakayama T. Epigenetic abnormalities of the mouse paternal zygotic genome associated with microinsemination of round spermatids. Dev Biol. 2006;289:195–205.
35. Zhou Q, Brown J, Kanarek A, Rajagopal J, Melton DA. In vivo reprogramming of adult pancreatic exocrine cells to beta-cells. Nature. 2008;455:627–32.
36. Takeuchi JK, Bruneau BG. Directed transdifferentiation of mouse mesoderm to heart tissue by defined factors. Nature. 2009;459:708–11.
37. Vierbuchen T, Ostermeier A, Pang ZP, Kokubu Y, Sudhof TC, Wernig M. Direct conversion of fibroblasts to functional neurons by defined factors. Nature. 2010;463:1035–41.
38. Ieda M, Fu JD, Delgado-Olguin P, Vedantham V, Hayashi Y, Bruneau BG, Srivastava D. Direct reprogramming of fibroblasts into functional cardiomyocytes by defined factors. Cell. 2010;142:375–86.
39. Tsuji H, Miyoshi S, Ikegami Y, Hida N, Asada H, Togashi I, Suzuki J, Satake M, Nakamizo H, Tanaka M, Mori T, Segawa K, Nishiyama N, Inoue J, Makino H, Miyado K, Ogawa S, Yoshimura Y, Umezawa A. Xenografted human amniotic membrane-derived mesenchymal stem cells are immunologically tolerated and transdifferentiated into cardiomyocytes. Circ Res. 2010;106:1613–23.
40. Bergmann O, Bhardwaj RD, Bernard S, Zdunek S, Barnabe-Heider F, Walsh S, Zupicich J, Alkass K, Buchholz BA, Druid H, Jovinge S, Frisen J. Evidence for cardiomyocyte renewal in humanso. Science. 2009;324:98–102.
41. Messina E, De Angelis L, Frati G, Morrone S, Chimenti S, Fiordaliso F, Salio M, Battaglia M, Latronico MV, Coletta M, Vivarelli E, Frati L, Cossu G, Giacomello A. Isolation and expansion of adult cardiac stem cells from human and murine heart. Circ Res. 2004;95:911–21.
42. Beltrami AP, Barlucchi L, Torella D, Baker M, Limana F, Chimenti S, Kasahara H, Rota M, Musso E, Urbanek K, Leri A, Kajstura J, Nadal-Ginard B, Anversa P. Adult cardiac stem cells are multipotent and support myocardial regeneration. Cell. 2003;114:763–76.
43. Matsuura K, Nagai T, Nishigaki N, Oyama T, Nishi J, Wada H, Sano M, Toko H, Akazawa H, Sato T, Nakaya H, Kasanuki H, Komuro I. Adult cardiac Sca-1-positive cells differentiate into beating cardiomyocytes. J Biol Chem. 2004;279:11384–91.
44. Martin CM, Meeson AP, Robertson SM, Hawke TJ, Richardson JA, Bates S, Goetsch SC, Gallardo TD, Garry DJ. Persistent expression of the ATP-binding cassette transporter, Abcg2, identifies cardiac SP cells in the developing and adult heart. Dev Biol. 2004;265:262–75.
45. Tateishi K, Ashihara E, Takehara N, Nomura T, Honsho S, Nakagami T, Morikawa S, Takahashi T, Ueyama T, Matsubara H, Oh H. Clonally amplified cardiac stem cells are regulated by Sca-1 signaling for efficient cardiovascular regeneration. J Cell Sci. 2007;120:1791–800.
46. Takehara N, Tsutsumi Y, Tateishi K, Ogata T, Tanaka H, Ueyama T, Takahashi T, Takamatsu T, Fukushima M, Komeda M, Yamagishi M, Yaku H, Tabata Y, Matsubara H, Oh H. Controlled delivery of basic fibroblast growth factor promotes human cardiosphere-derived cell engraftment to enhance cardiac repair for chronic myocardial infarction. J Am Coll Cardiol. 2008;52:1858–65.

J Artif Organs (2011) 14:215–222
DOI 10.1007/s10047-011-0568-6

ORIGINAL ARTICLE

Efficient transfection method using deacylated polyethylenimine-coated magnetic nanoparticles

Daisuke Kami · Shogo Takeda · Hatsune Makino · Masashi Toyoda · Yoko Itakura · Satoshi Gojo · Shunei Kyo · Akihiro Umezawa · Masatoshi Watanabe

Received: 6 October 2010 / Accepted: 31 March 2011 / Published online: 3 May 2011

Abstract Low efficiencies of nonviral gene vectors, such as transfection reagent, limit their utility in gene therapy. To overcome this disadvantage, we report on the preparation and properties of magnetic nanoparticles [diameter (d) = 121.32 ± 27.36 nm] positively charged by cationic polymer deacylated polyethylenimine (PEI max), which boosts gene delivery efficiency compare with polyethylenimine (PEI), and their use for the forced expression of plasmid delivery by application of a magnetic field. Magnetic nanoparticles were coated with PEI max, which enabled their electrostatic interaction with negatively charged molecules such as plasmid. We successfully transfected 81.1 ± 4.0% of the cells using PEI max-coated magnetic nanoparticles (PEI max-nanoparticles). Along with their superior properties as a DNA delivery vehicle, PEI max-nanoparticles offer to deliver various DNA formulations in addition to traditional methods. Furthermore, efficiency of the gene transfer was not inhibited in the presence of serum in the cells. PEI max-nanoparticles may be a promising gene carrier that has high transfection efficiency as well as low cytotoxicity.

Keywords Deacylated polyethylenimine · Magnetic nanoparticle · Efficient nonviral transfection method

D. Kami
Innovative Integration between Medicine and Engineering Based on Information Communications Technology, Yokohama National University Global COE Program, Yokohama, Japan
e-mail: dkami@tmig.or.jp

S. Takeda · M. Watanabe (✉)
Laboratory for Medical Engineering, Division of Materials and Chemical Engineering, Yokohama National University, 79-1 Tokiwadai, Hodogaya-ku, Yokohama 240-8501, Japan
e-mail: mawata@ynu.ac.jp

D. Kami · H. Makino · M. Toyoda · A. Umezawa
Department of Reproductive Biology, National Institute for Child Health and Development, Tokyo, Japan

D. Kami · M. Toyoda (✉) · Y. Itakura · S. Gojo
Vascular Medicine, Research Team for Geriatric Medicine, Tokyo Metropolitan Institute of Gerontology, 35-2 Sakae-cho, Itabashi-ku, Tokyo 173-0015, Japan
e-mail: mtoyoda@tmig.or.jp

S. Gojo · S. Kyo
Division of Therapeutic Strategy for Heart Failure, Department of Cardio-Thoracic Surgery, The University of Tokyo, Tokyo, Japan

Introduction

Nanotechnologies that allow the nondisruptive introduction of carriers in vivo have wide potential for gene and therapeutic delivery systems [1–4]. Extremely small particles have been successfully introduced into living cells without any further modification to enhance endocytic internalization, such as for cationic help. The cells containing the internalized nanoparticles continued to thrive, indicating that the particles have no inhibitory effect on mitosis. Therefore, iron oxide magnetic nanoparticles have played an important role as magnetic resonance imaging contrast agents [5, 6], and cytotoxicity of this nanoparticle was none (or low) [7, 8]. Thereby, the functionalized iron oxide magnetic nanoparticles are expected to be useful as a new gene delivery tool [3].

Cationic polymer polyethylenimine (PEI) (linear, MW 25,000) is known as the transfection reagent in molecular biology [9], and the dispersant in nanotechnology [10]. PEI are configured to form the positively charged complex with DNA, which binds to anionic cell surface residues and

enter the cell via endocytosis [9, 11], keeping the dispersed state in the solution [10]. However, PEI containing residual *N*-acyl groups is a disadvantage for transfection efficiency. Also, the deacylated PEI (PEI max) for transfection reagent was reported, showing an increase in optimal transfection efficiency of 21-fold in comparison with PEI [12].

The transfection method using magnetic nanoparticles utilizes a magnetic force to deliver DNA into target cells. Therefore, the plasmid is first associated with magnetic nanoparticles. Then, the application of a magnetic force drives the plasmid–nanoparticle complexes toward and into the target cells, where the cargo is released (Fig. 1a) [13–16]. The magnetic nanoparticles are also coated with biological polymers, such as PEI, to allow plasmid loading (Fig. 1b). The binding of the negatively charged plasmid to the positively charged PEI max-coated magnetic nanoparticles (PEI max-nanoparticles) occurs relatively quickly. After complex formation, the loaded nanoparticles are incubated together with the target cells on a magnet plate. Owing to the magnetic force, the iron particles are rapidly drawn toward the surface of the cell membrane. Cellular uptake occurs by either endocytosis or pinocytosis [17]. Once delivered to the target cells, the plasmid is released into the cytoplasm [17, 18]. The magnetic nanoparticles accumulate in endosomes and/or vacuoles [18]. Over time, the nanoparticles are degraded and the iron enters normal iron metabolism [19]. An influence of magnetic nanoparticles on cellular functions has not been reported yet. However, in most cases, the increased iron concentration in culture media does not lead to cytotoxic effects [7].

In this study, we coated the transfection reagent, PEI max, on the surface of magnetic nanoparticles and applied a gene vector using PEI max-nanoparticles for a highly efficient transfection method. Our results indicate a high level of expression of the transfected gene in living cells using the plasmid-conjugated PEI max-nanoparticles.

Materials and methods

Materials

Magnetic nanoparticles (γ-Fe_2O_3, $d = 70$ nm) were purchased from CIK NanoTek. PEI max linear (MW 25,000) was purchased from Polysciences Inc. FuGENE HD was purchased from Roche Diagnostics. Deionized water was purchased from Gibco. Magnetic sheet (160 mT), and neodymium magnet (130 mT) was purchased from Magna Co. Ltd.

Preparation of the PEI max-nanoparticles

The magnetic nanoparticles (1.0 g) were dissolved in 30 ml of PEI max solution (1.6 mg PEI max/ml). The mixture was sonicated for 2 min (40 W) on ice, and 20 ml of deionized water was added (final concentration 1.0 mg PEI max/ml). The ferrofluid was centrifuged at 4,100×*g* for 5 min. The supernatant fluids were harvested and transferred into a fresh tube. This fluid was washed twice by deionized water and resolved into an equal volume of the PEI max solution (1.0 mg PEI max/ml). Magnetic nanoparticles in this fluid

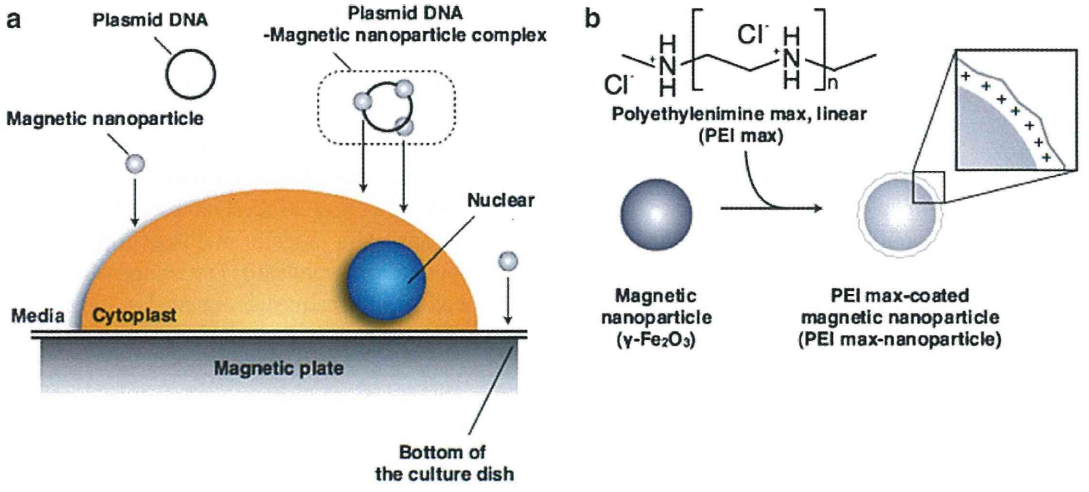

Fig. 1 Nanoparticle transfection method and cationic coating: **a** Plasmid-conjugated magnetic nanoparticles moved to the cell surface on the magnetic sheet upon application of magnetic force. Then, the magnetic force drove this complex toward and into the target cells. **b** Magnetic nanoparticles (γ-Fe_2O_3, $d = 70$ nm) (CIK NanoTek Inc.) were coated with deacylated polyethylenimine max linear (PEI max) (MW 25,000) (Polysciences Inc.), known as a dispersive agent, and transfection reagents. The surface of the PEI max-nanoparticle was positively charged. Nanoparticles and plasmid formed complexes by ionic interaction of the negatively charged plasmid and the positively charged surface of the PEI max-nanoparticle

were coated with PEI max and dispersed in PEI max solution or deionized water.

Measurement of PEI max-nanoparticle size and ζ-potential

The size of the PEI max-nanoparticles was measured with a laser light-scattering method using a fiberoptics particle analyzer (FPAR-1000, Otsuka Electronics). The measurement was performed in triplicate, and median size and range of size distribution were obtained. The ζ-potential of the PEI max-nanoparticles was determined with electrophoretic light-scattering spectrophotometer (ELSZ-2, Otsuka Electronics).

Charge characteristics of PEI max-nanoparticle

PEI max-nanoparticle (100 μg) and each weight of plasmid (2,000, 1,000, 750, 500, 375, 250, 188 ng) were mixed in deionized water or PEI max solution (1 mg/ml). Each solution were reacted for 1 h at room temperature.

Plasmid DNA was bound to PEI max-nanoparticles

Plasmid DNA (5 μg) was reacted with various weights of PEI max-nanoparticles (0–1.8 mg/tube) in deionized water for 15 min at room temperature. Then, the reaction mixtures were centrifuged at 12,000×*g* for 15 min and were formed in a sol-like precipitation in the lower layer. The concentration of DNA in the upper layer (hyaline layer) was determined by NanoDrop 1000 spectrophotometer (Thermo Scientific). The relative concentration of plasmid DNA treated without PEI max-nanoparticles was regarded as 100%.

Cell culture

P19CL6 cells (CL6 cells) from a mouse embryonic carcinoma cell line were grown on 100-mm dishes (Becton-Dickinson) in alpha-minimum essentioal medium (MEM) (Nacalai Tesque) supplemented with 10% fetal bovine serum (FBS) (JRH Bioscience Inc.), penicillin, and streptomycin (Gibco), and were maintained in a 5% carbon dioxide (CO_2) atmosphere at 37°C.

Transfection procedure using PEI max-nanoparticles

CL6 cells were seeded at 1×10^5 cells/well in six-well plates (Becton-Dickinson) 18 h before transfection. Immediately before transfection, cells were rinsed and supplemented with fresh culture medium (1 ml). The PEI max-nanoparticles (in 1 mg PEI max/ml solution) were mixed with 2.0 μg of the plasmid [pCAGGS–enhanced green fluorescent protein (EGFP), the modified pCAGGS expression vector [20], weight ratio PEI max:plasmid = 3:1] and incubated in the deionized water at final volume of 50 μl at room temperature for 15 min. The complexes were added to the CL6 cells on a magnetic sheet various times (0, 0.5, 1, 4, and 24 h). Forty-eight hours after transfection, CL6 cells were evaluated; 1 mg/ml of PEI max solution was used as a positive control.

Quantitative real-time reverse transcriptional (RT)-PCR

Total RNAs from CL6 cells were extracted using ISOGEN (Nippon Gene). To perform quantitative real-time polymerase chain reaction (PCR) assay, total RNA (1 μg) was reverse-transcribed using random hexamer and the PrimeScript RT reagent kit (TaKaRa). Quantitative real-time reverse transcriptional (RT)-PCR was performed on LineGene (BioFlux), using 100 ng of complementary DNA (cDNA) in 25 μl reaction volumes with 10 nmol/l EGFP primer and 12.5 μl of SYBR Premix Ex Taq (TaKaRa). PCR primers for the gene of EGFP and *Gapdh* were designed to amplify each cDNA using the sense primer (5′-CCGACCACATGAAGCAGCAC-3′) and the reverse primer (5′-CTTCAGCTCGATGCGGTTCAC-3′) for the EGFP, and the sense primer (5′-TGCGACTTCAACAGCA ACTC-3′) and the reverse primer (5′-CTTGCTCAGTGTC CTTGCTG-3′) for the *Gapdh*. Calculations were automatically performed by fluorescent quantitative detection system software (BioFlux).

Nanoparticle cytotoxicity

Alamar Blue [21] was used to measure cell proliferation and metabolic activity as an oxidation-reduction indicator. After 48 h of PEI max or PEI max-nanoparticle exposure, 900 μl of medium from each condition was transferred into a 24-well flat-bottomed plate. One hundred microliters of Alamar Blue (AbD Serotec) was added to each well, and the well plate was incubated for 3 h at 37°C. Fluorescence was measured at 570/600 nm in a Viento multispectrophotometer reader (Dainippon Pharmaceutical). The relative absorbance of CL6 cells without any treatment is regarded as 100% (it is indicated as a percent control in Fig. 4c).

Flow cytometric analysis

To count the numbers of EGFP-positive cells using PEI max-nanoparticles (0.8 μg/well in a six-well plate) on a magnetic sheet for 4 h (PEI max alone as a positive control), a Cytomics FC500 (Beckman Coulter Inc.) was used, and data were analyzed with FlowJo Ver.7 (Tree Star Inc.). Each sample was compared with negative control cells (without treatment).

Statistical analysis

Results, shown as the mean ± standard error (SE), were compared by analysis of variance (ANOVA) followed by Scheffe test (http://chiryo.phar.nagoya-cu.ac.jp/javastat/JavaStat-j.htm), with $P < 0.05$ considered significant.

Results

Characterization of PEI max-nanoparticles

Magnetic nanoparticles were well coated with PEI max and were highly dispersed in PEI max solution (1 mg/ml) or deionized water. Secondary size of the PEI max-nanoparticles was approximately 121.32 ± 27.36 nm (Fig. 2A). To evaluate stability in PEI max solution (1 mg/ml) or deionized water, we measured the ζ-potential of PEI max-nanoparticles, which was +45.53 mV in PEI max solution and +30.05 mV in deionized water. The PEI max-nanoparticles were aggregated by magnetic force (Fig. 2Ba) and quickly redispersed by vortex (Fig. 2Bb). Time-lapse photography (30 s/s) shows that magnetic nanoparticles were gradually removed at the site of the neodymium magnet (right side of the tube) for 2 h (magnetic nanoparticles for transfection: http://www.youtube.com/watch?v=Hyjfc4moHK4). These nanoparticles in PEI max solution were not aggregated without magnetic force. To avoid aggregation of plasmid-attached PEI max-nanoparticle caused by charge neutralization, it was necessary that their weight ratio was approximately 1:400 (Fig. 2C). In general, 1–2 μg of plasmid per well was mixed with the transfection reagent such, as PEI max, and FuGENE HD into six-well plates. However, too much (400–800 μg of nanoparticle per well) caused inhibition of transfection (described later). To solve the problem, we decided to use in 1 mg/ml of PEI max solution as a solvent. As a result, each concentration of the plasmid did not aggregate with PEI max-nanoparticle (Fig. 2Bb). To evaluate whether the plasmid DNA was attached to PEI max-nanoparticles in deionized water, we reacted PEI max-nanoparticles with plasmid DNA for 15 min at room temperature. Measuring the concentration of plasmid DNA in the upper layer (hyaline layer), the weight of PEI max-nanoparticles was reduced in a dependent manner (Fig. 2D).

Transfection efficiency using PEI max-nanoparticles and magnetic sheet, and viability of the CL6 cells treated with PEI max-nanoparticles

CL6 cells were transfected with pCAGGS-EGFP and PEI max alone as a positive control (Fig. 3a) and pCAGGS-EGFP and PEI max-nanoparticles (Fig. 3b) at 48 h after transfection. Many EGFP-positive cells were observed among CL6 cells transfected with PEI max-nanoparticles compared with those transfected with PEI max. To evaluate the optimum condition of transfection using PEI max-nanoparticles, quantitative real-time RT-PCR was performed at 48 h after transfection. The optimum condition of transfection was a concentration of 0.8 μg/well (Fig. 4a) on a magnetic sheet for 4 h (Fig. 4b). *EGFP* gene expression level was reduced under transfection of excess magnetic nanoparticles (7.5 μg/well) (Fig. 4a) and prolonged time on the magnetic sheet (24 h) (Fig. 4b). EGFP expression in CL6 cells transfected with PEI max-nanoparticles was increased approximately two to fourfold compared with those transfected with PEI max. The viability of CL6 cells treated with PEI max-nanoparticles, as measured by Alamar Blue assay, did not differ between cells treated with/without PEI max alone (Fig. 4c).

Number of EGFP-positive cells by flow cytometric analysis

Forty-eight hours after transfection using PEI max alone or PEI max-nanoparticles, we examined the number of EGFP-positive cells (total 10,000 cells) by flow cytometric analysis. Compared with the negative control (untreated CL6 cells), 42.2 ± 8.5% of cells treated with PEI max alone (Fig. 5a), 81.1 ± 4.0% of cells treated with 0.8 μg of PEI max-nanoparticles per well on the magnetic sheet for 4 h (Fig. 5b), and 13.9 ± 1.1% of cells treated with FuGENE HD (Fig. 5c) expressed EGFP. The number of EGFP-positive cells was significantly increased (approximately twofold) using PEI max-nanoparticles.

Discussion

In this study, to express target gene with high efficiency and low cytotoxicity, we focused on PEI max and magnetic nanoparticles (γ-Fe_2O_3). Many researchers have reported various transfection methods using PEI and magnetic nanoparticles, such as γ-Fe_2O_3, and superparamagnetic iron oxide nanoparticle (used as magnetic resonance imaging contrast agents) (Table 1). However, these methods had a low transfection efficiency [14, 15], combined with virus (adenovirus, or retrovirus) [15], and high cytotoxicity (low cell viability) [13] and may therefore have little effectiveness for clinical use.

The expression level of the *EGFP* gene was reduced under transfection of excess magnetic nanoparticles (7.5 μg/well) (Fig. 4a). This result may indicate that a high concentration of PEI max-nanoparticles formed the large agglutinate complexes with plasmid DNAs [22, 23]